buildings

MDPI

Article

Investigation on the Flow and Thixotropic Properties of Alkali-Activated Concrete

Jian Zhang [1,2,3,4], Yufei Liu [1,2,3,4], Jin Zhu [1,2,3,4], Jinhui Liu [1,2,3,4], Yuefeng Ma [5], Shengtian Zhai [6] and Yubo Sun [7,*]

[1] State Key Laboratory of Intelligent Geotechnics and Tunnelling, Shenzhen University, Shenzhen 518060, China
[2] Key Laboratory of Coastal Urban Resilient Infrastructures (Shenzhen University), Ministry of Education, Shenzhen 518060, China
[3] National Engineering Research Center of Deep Shaft Construction, Shenzhen University, Shenzhen 518060, China
[4] College of Civil and Transportation Engineering, Shenzhen University, Shenzhen 518060, China
[5] College of Materials Science and Engineering, Chongqing University, Chongqing 400045, China
[6] School of Civil Engineering and Architecture, Henan University of Science and Technology, Luoyang 471023, China
[7] Department of Civil and Environmental Engineering, The Hong Kong Polytechnic University, Hong Kong 999077, China
* Correspondence: yubo.sun@polyu.edu.hk

Abstract: Alkali-activated materials (AAMs) offer an eco-friendly alternative to traditional Portland cement, yet their rheological properties, particularly in concrete mixtures, remain largely underexplored. This study conducted rheological tests to investigate the flow properties and thixotropic behavior of alkali-activated slag (AAS) concrete with varying water-to-binder (w/b) ratios and silicate modulus (Ms). The thixotropy of AAS concrete was assessed using the thixotropic index, breakdown area, and variations in apparent viscosity under different shear rates, revealing correlations between thixotropic behaviors and rheological parameters. Mixtures with lower Ms and w/b ratios showed limited slump values and rapid structural build-up due to increased interparticle connections. As Ms increased, enhanced thixotropic behaviors were observed, attributed to the rapid formation of early hydration products. This led to a significant increase in peak torque values and a slight decrease in equilibrium torque values at various rotational speeds. In turn, AAS concrete with higher Ms demonstrated improved fluidity and workability retention after thixotropic build-up was erased. The results of this study provide valuable insights into the flow and thixotropic behaviors of fresh AAS concretes for practical applications.

Keywords: alkali-activated slag concrete; rheology; thixotropy; structural build-up; breakdown

Citation: Zhang, J.; Liu, Y.; Zhu, J.; Liu, J.; Ma, Y.; Zhai, S.; Sun, Y. Investigation on the Flow and Thixotropic Properties of Alkali-Activated Concrete. *Buildings* **2024**, *14*, 4085. https://doi.org/10.3390/buildings14124085

Academic Editor: Grzegorz Ludwik Golewski

Received: 21 November 2024
Revised: 19 December 2024
Accepted: 22 December 2024
Published: 23 December 2024

1. Introduction

In the pursuit of sustainable construction, alkali-activated materials (AAMs) have been widely studied as potential replacements for Portland cement (PC) [1–3]. Compared with PC, AAMs not only reduce greenhouse gas emissions [4–6] but also provide better mechanical properties [7,8] and potentially superior resistance to chemicals and fire [9]. However, the fundamental mechanism of governing rheology in AAMs is still poorly understood, with limited exploration in the literature. Challenges like a rapid reduction in slump, increased viscosity, and uncontrolled setting times are commonly observed, particularly in AAMs containing a high proportion of silicate [10,11]. The rheology of AAMs might be affected by various parameters, including the properties of precursors, the composition of activators, and the volume fraction in the system [12]. The complex dissolution kinetics of precursors and the interaction among multiple phases have resulted in distinctive rheological behavior in AAMs, where the colloidal interparticle interactions are dissipated by the highly viscous activator solution [11,13]. Further, the conventional chemical admixtures for PC are incompatible with AAMs, and thereby cannot improve the

fluidity [14,15]. So far, most studies on the rheology of AAMs have primarily concentrated on the paste and mortar scales. Instead, the rheological behavior of AAM concrete was only discussed in a few studies [12,16,17]. Accordingly, the wide application of AAM concrete in the construction industry has progressed slowly due to technical obstacles and the absence of regulations.

As advanced concrete technologies develop, the thixotropic characteristics of freshly prepared cementitious mixtures have become a focal point of interest in recent years [18–20]. The significance of concrete thixotropy lies in its strong connection with the initial stiffening phase during extrusion or construction. Thixotropic behavior was first introduced by the group of Herbert Freundlich about a hundred years ago, which describes a reversible process in which the viscosity progressively reduces when applying shear stress and gradually recovers as the stress is removed [21]. For cementitious materials, thixotropy is normally expressed by a partially reversible structural build-up at rest and a structural breakdown under external shear stress [22]. It appears to be more complicated as the particle interaction permanently evolves along the hydration process [23]. Specifically, the structural development of the cement mixture primarily results from colloidal agglomeration among solid particles and reaction products at the points of local contact [24]. The shear energy intensity applied determines whether the structure can partially recover, breaking interparticle bonds and enabling dispersed particles to reconnect through newly generated hydration products as the reaction progresses [18]. Conversely, the accumulation of reaction products constantly reinforces the local interparticle bonds. During prolonged resting periods, irreversible structuration can develop because connections between cement particles are too rigid to be disrupted by the mixing force [18,25].

The thixotropic properties of PC have been the subject of considerable research. The influence of mix design parameters, mineral admixtures, and chemical additives has been thoroughly explained to clarify the formation and breakdown of thixotropic structures in fresh concrete [18,19,24,26]. Furthermore, understanding thixotropic behavior has proven beneficial in assessing time-dependent concrete performance aspects, such as static stability [27], formwork pressure variation [28,29], permeability [30], interlayer bonding in multilayer casting [31], and construction rates in 3D printing [32,33]. Conversely, the rheology and thixotropic behavior of alkali-activated materials (AAMs) have received limited attention in the existing literature, despite their critical role in determining the workability, stability, and performance of these materials in various applications. Most investigations have only provided brief assessments, often restricted to studies focused on paste-level compositions, which typically involve simple systems with controlled variables. This narrow focus has left a significant gap in understanding their behavior in more complex systems, such as those incorporating aggregates, fibers, or other additives, as well as in practical applications where external factors like temperature, humidity, and mixing conditions can significantly influence material properties.

This study aims to expand our knowledge of the rheology of AAS pastes and extend it into concrete mixtures, offering insights into the flow and thixotropic properties of AAS concrete by varying the water-to-binder (w/b) ratio and silicate modulus (Ms) in activators. To assess the fresh properties, slump, stress growth, and flow curve tests were conducted, and thixotropy was measured through multiple methods, such as calculating the thixotropic index from rheological data and analyzing the breakdown area and viscosity reduction at different shear speeds. Efforts were made to establish correlations between thixotropy measured by various methods. In addition, reaction kinetics were studied with calorimetry to better understand the evolution of fresh properties. The results from this study may offer an enhanced understanding of the flow properties and thixotropic behavior, assisting in large-scale utilizations of AAS concrete.

2. Experimental Method

2.1. Materials

Ground granulated blast furnace slag (BFS) with a relative density of 2.89 g/cm^3 was used in this work. Chemical compositions of BFS measured with X-ray fluorescence (XRF) are shown in Table 1, and the oxide percentages were calculated by assuming all elements exist in their primary oxide forms. The particle size distribution and morphology of BFS are illustrated in Figures 1a and 1b, respectively.

Table 1. Chemical composition of BFS (wt. %).

CaO	SiO_2	Al_2O_3	MgO	Na_2O	K_2O	SO_3	TiO_2	Fe_2O_3	MnO	ZrO_2	LOI [a]	Other
40.90	30.10	13.70	9.07	0.65	0.60	2.40	1.35	0.36	0.35	0.14	0.08	0.38

[a] LOI measured by TG analysis at 950 °C.

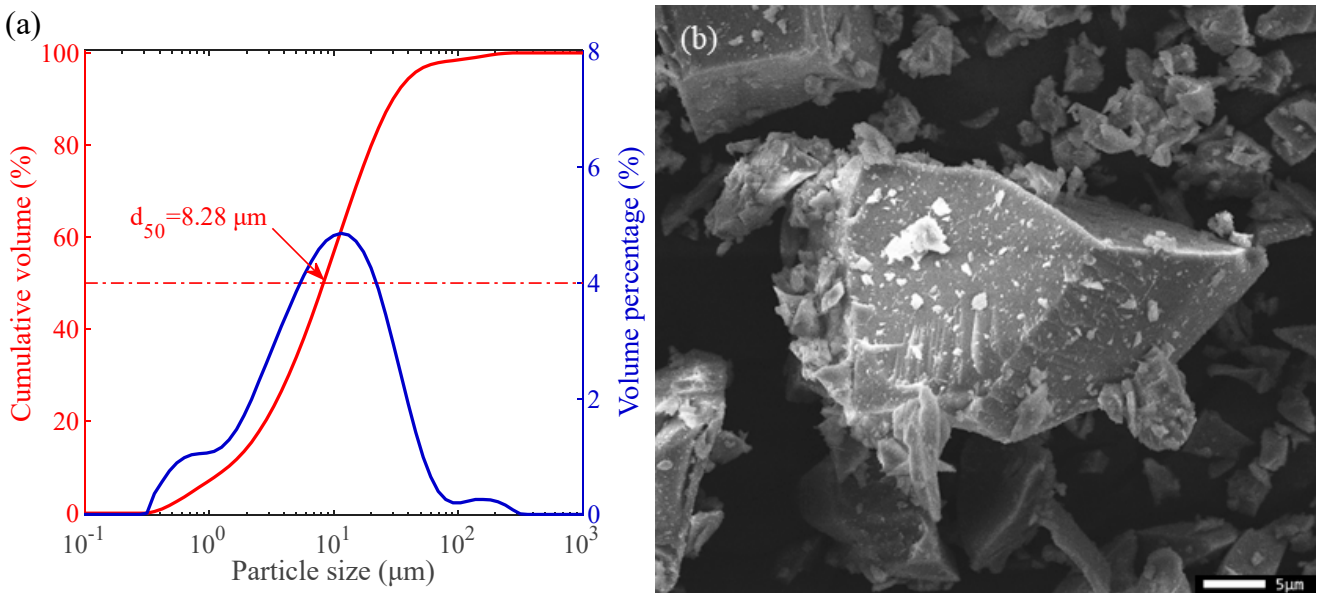

Figure 1. BFS physical characteristics. (**a**) Particle size distribution by laser diffraction. (**b**) Surface morphology by SEM.

Reagent-grade anhydrous sodium hydroxide pearls and the sodium silicate solution comprising 15% Na_2O, 30% SiO_2, and 55% water were employed to synthesize activator solutions. River sand and gravel were employed to produce AAS concrete, and their water absorption and specific gravities are shown in Table 2. It should be noted that all aggregates used in this study were oven-dried at 105 °C for 24 h to eliminate the moisture content before use in concrete.

Table 2. Water absorption and specific gravity of aggregates.

Aggregate	Sand	Coarse 1	Coarse 2
Particle fraction	0–4 mm	2–8 mm	8–16 mm
Water absorption (%)	0.33	0.65	0.55
Specific gravity	2.65	2.64	2.67

2.2. Mixture Proportions

Table 3 illustrates the mixture proportions of AAS concrete. Nine blends were prepared with a consistent precursor dose of 400 kg/m^3. The activators were formulated to maintain a constant sodium concentration, equivalent to 4% Na_2O by the mass of the precursor [34], with the water-to-binder (w/b) ratio of AAS concrete varying between 0.4 and 0.5 to achieve

suitable consistency. The water absorption of dried aggregates was compensated by extra water content calculated by the absorption rate shown in Table 2. As indicated in Table 3, Ms values used in activators ranged from 0.25 to 0.75, since either lower or higher Ms values have led to flash setting in preliminary tests. Activators were prepared by dissolving sodium hydroxide and sodium silicate solution in tap water 24 h before mixing. Aggregate gradation in the mixtures was structured to lie between the A16 and B16 curves as specified by DIN 1045-2.

Table 3. Mix design of AAS concretes.

Mix	BFS (kg/m^3)	Activator				w/b *	Aggregate (kg/m^3)		
		Sodium Hydroxide (kg/m^3)	Sodium Silicate (kg/m^3)	Ms	Extra Water (kg/m^3)		0–4 mm	2–8 mm	8–16 mm
A1	400	18.06	13.33	0.25	162.29	0.40	715	491	583
A2					183.50	0.45	692	476	565
A3					204.70	0.50	670	460	547
A4		15.48	26.67	0.50	156.33	0.40	712	490	581
A5					177.70	0.45	689	474	563
A6					199.08	0.50	667	458	544
A7		12.90	40.00	0.75	150.36	0.40	709	488	579
A8					171.91	0.45	686	472	560
A9					193.45	0.50	664	456	542

* Refers to the total water content, including that from the activator and any additional water, divided by the sum mass of the precursor and solid activators.

2.3. Sample Preparation

AAS mixtures in this study were prepared at both paste and concrete levels. AAS pastes were created according to the mix design shown in Table 3, excluding aggregates, using a handheld mixer for calorimetry tests. The mixing protocol was consistent with that used for concrete mixes, as described below. AAS concretes were prepared in 30-L batches following standard procedures. Initially, BFS and aggregates were dry-mixed for 2 min in a planetary mixer. The activator solution was then gradually added over 30 s, followed by 3 additional minutes of mixing to achieve fresh mixtures.

2.4. Testing Program

2.4.1. Isothermal Calorimetry

Reaction kinetics were studied using a TAMAIR isothermal calorimeter. About 14 g of fresh paste was loaded in a sealed glass ampoule. These ampoules, containing the fresh AAS paste, were then placed in the isothermal channels for calorimetry testing. Heat evolution was monitored at 20 ± 0.5 °C over 24 h. The heat flow and cumulative heat release were normalized to 1 g of solid binder, encompassing both precursors and solid activators. Calorimetry tests were conducted twice to confirm repeatability.

2.4.2. Flow Properties

An ICAR Plus rheometer was employed to perform stress growth and flow curve tests, determining the rheological characteristics of AAS concrete. The geometry of the testing setup is schematically displayed in Figure 2. About 20 L of fresh AAS concrete were loaded into the container for rheological measurements, with the rest reserved for slump tests. Before each testing age, the concrete was remixed for 60 s to ensure a reference state among different samples [35]. After inserting the rheometer vane, the concrete was allowed to rest for approximately 1 min to release undissipated energy.

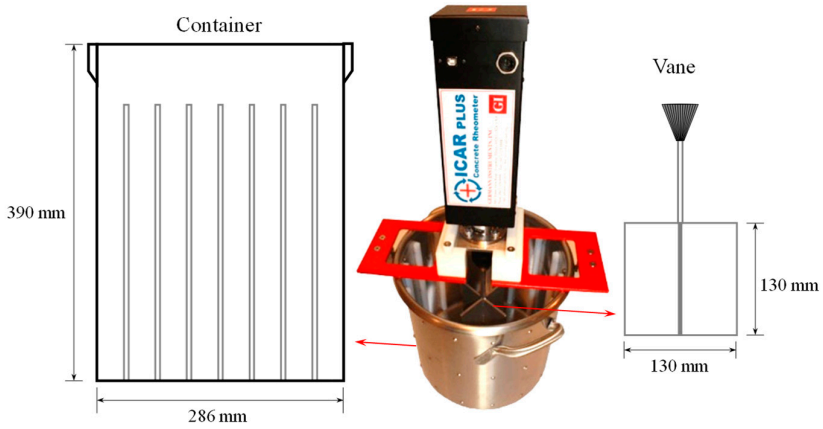

Figure 2. Geometry of the rheometer setup.

Rheological tests, including stress growth and flow curve steps, commenced approximately 5 min after the initial contact between the precursor and activators. The stress growth test was conducted at 0.025 rps for 60 s, with torque measurements recorded over time. The static yield stress of AAS concrete was determined using the peak torque observed during the stress growth test, as described by Equation (1) [36].

$$\tau_s = \frac{2T}{\pi {d_v}^3 \left(\frac{h_v}{d_v} + \frac{1}{3}\right)} \quad (1)$$

where τ_s represents the static yield stress in Pa, T represents the maximum torque in Nm, d_v represents the vane's diameter in m, and h_v represents the vane's height in m.

The fresh AAS concrete was allowed to rest for 1 min before conducting the flow curve test. This was followed by a pre-shear at 0.5 rps for 30 s to eliminate structuration. Shear steps were then applied with progressively increasing and decreasing rotational speeds, ranging from 0.05 to 0.5 rps in six steps. Each step lasted 30 s, and the average torque from the last 10 s was calculated to represent the equilibrium state. The downward portions of the torque-rotational speed curve were linearly fitted using the Bingham model, while dynamic rheological parameters were derived from the Reiner–Riwlin equations [37]. The rheometer vane was removed after flow curve tests, and any mortar attached to the vane blade was returned to the rheometer container to prevent material loss. The container was then covered with plastic sheets to prevent moisture evaporation.

Stress growth measurements were repeated every 15 min until one hour on the same batch of AAS concrete to assess the structural build-up progress. The initial stress growth test was marked as '0 min' (i.e., 5 min after the first contact between precursor and activators). In the meantime, slump tests were performed simultaneously every 15 min with an Abrams cone according to EN 12350-2 to evaluate the workability retention [16].

2.4.3. Tests on Thixotropic Behaviors

Tests on concrete thixotropy were performed with new batches of concrete to avoid the influence of shear history and time-dependent behaviors. Given the high early reactivity of AAS mixtures [38], thixotropic properties were assessed on the basis of 5 min intervals for structuration using the methods described below:

The first approach focused on calculating the thixotropic index of AAS concrete by measuring the maximum and steady-state shear stresses during the stress growth test with a low shear rate (0.025 rps) [16]. Following 1 min of remixing, the fresh concrete underwent a 5 min structuration period. A typical profile of a stress growth test is illustrated in Figure 3a, showing the torque peaking after an initial steep rise, indicating the gradual breakdown of particle interactions while initiating the flow of fresh concrete. Once the static mixture yielded, the torque slowly decreased until a steady state was reached, indicating the energy

needed to sustain the dynamic flow. The maximum torque and the average torque over the final 10 s were utilized to calculate the peak shear stress τ_0 and the equilibrium shear stress τ_e, respectively. Using Equation (1), shear stresses were determined from the torque values detected, and the thixotropic index (T_I) was calculated by Equation (2) [28,39].

$$T_I = (\tau_0 - \tau_e)/\tau_e \quad (2)$$

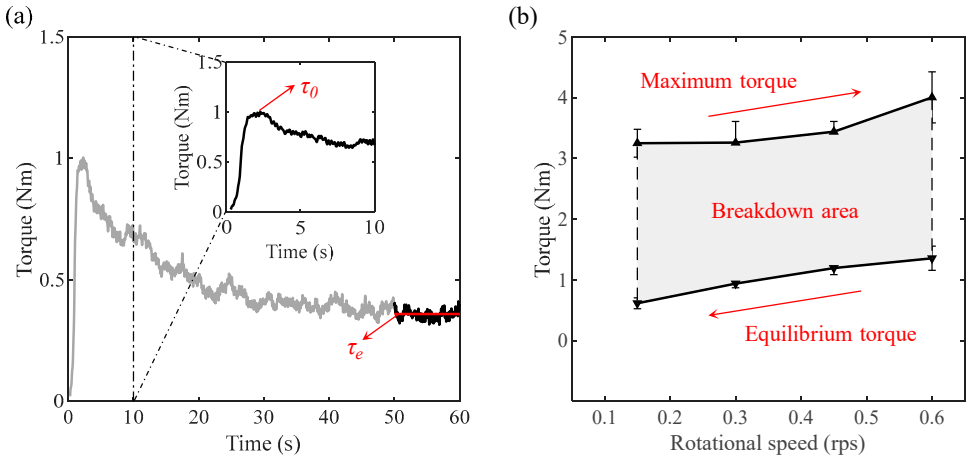

Figure 3. Determination of thixotropic behaviors in AAS concretes (depicted with A9). (**a**) Profile of torque development derived from a stress growth test. (**b**) Breakdown area derived from various rotational speeds.

The breakdown area was evaluated at different rotational speeds within higher shear rate regions (0.15–0.6 rps) to study thixotropic properties [26,39]. After 1 min of remixing and a 5 min rest, AAS concrete was subjected to a 30 s shear process at 0.15 rps to reach a steady state. The cycle consisting of a 5 min rest followed by high shear rate steps was repeated at increased rotational speeds of 0.3, 0.45, and 0.6 rps. The maximum torque occurring at each speed was labeled as T_m, while the equilibrium torque (T_e) was calculated from the average torque during the last 10 s. The breakdown area was then determined as the space between the curves of maximum and equilibrium torque across different shear speeds, as shown in Figure 3b.

On top of that, the thixotropy of AAS concretes was further assessed by measuring the reduction in apparent viscosity (Δ_{app}) at different rotational speeds, as proposed by Assaad and Khayat [29,39]. Δ_{app} was expressed as the difference between the initial and equilibrium torque values, divided by the corresponding rotational speed, as indicated in Equation (3) [26].

$$\Delta_{app} = (T_0 - T_e)/N$$

3. Results and Discussion

3.1. Reaction Kinetics

The normalized heat flow and cumulative heat evolution of AAS pastes are depicted in Figure 4. In the Ms0.25 group, no distinct induction period was observed during the early activation reactions. The acceleration phase commenced immediately following the initial dissolution peak, with the peak heat flow reaching 1.79 mW/g approximately 2 h after the precursors were in contact with activators in A1. Increasing the w/b ratio from 0.4 to 0.45 in A2 resulted in a 25 min delay in the acceleration peak and a 15.1% decrease in heat flow intensity. Further increasing the w/b ratio to 0.5 in A3 delayed the maximum heat flow by 36 min and reduced it by 20.7%. These findings suggest that a higher w/b ratio slightly decreased the exothermic reactions in Ms0.25 mixtures. Moreover, A1, A2, and A3 exhibited similar trends in cumulative heat evolution, with two major increments

corresponding to the dissolution and acceleration peaks in heat flow curves. After 24 h, the cumulative heat of A1 reached 52.83 J/g. A higher w/b ratio led to less intense exothermic reactions in A2 and A3, with their cumulative heat release reduced by 6.4% and 11.8% compared to A1, respectively.

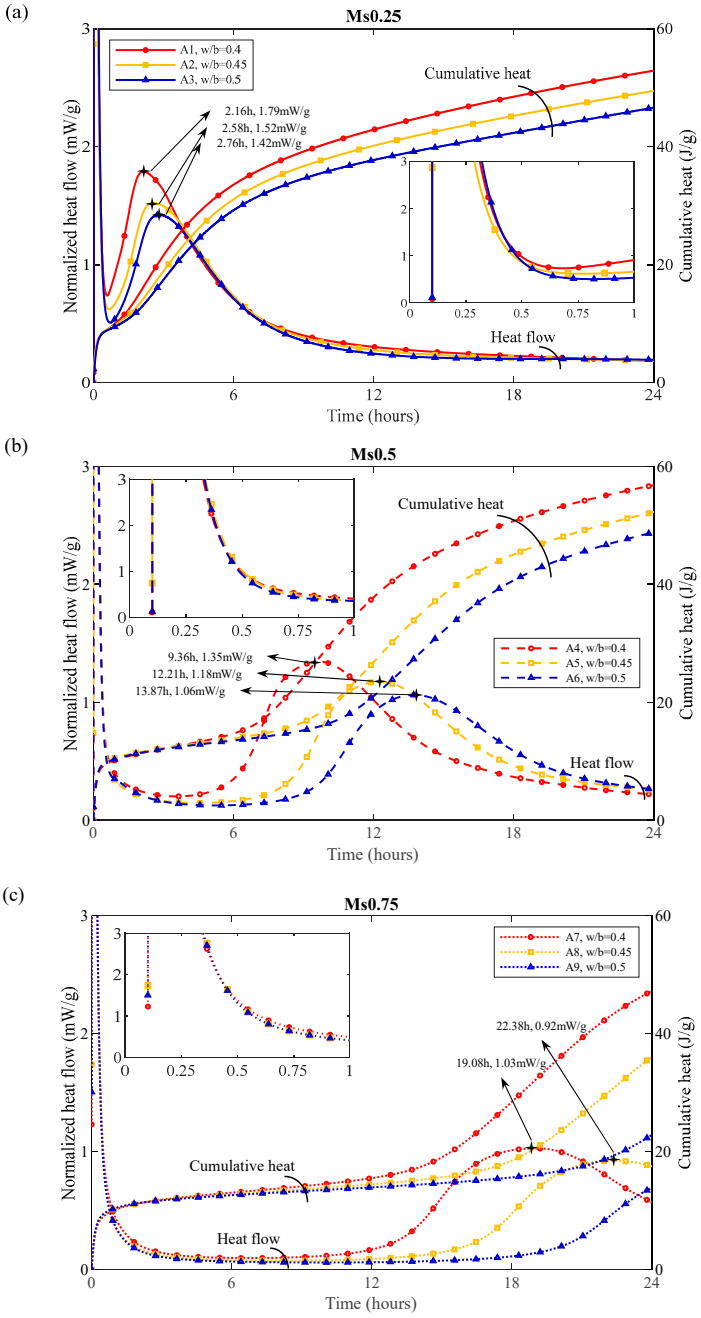

Figure 4. Normalized heat flow and cumulative heat evolution of AAS paste: (**a**) Ms0.25 mixtures (A1, A2, and A3); (**b**) Ms0.5 mixtures (A4, A5, and A6); and (**c**) Ms0.75 mixtures (A7, A8, and A9).

As depicted in Figure 4b, an evident induction period followed the initial dissolution phase as Ms increased in A4, A5, and A6, becoming more pronounced in Ms0.75 mixtures (Figure 4c). This suggests that the addition of extra silicate species from the activator significantly retarded reaction kinetics. Furthermore, mixtures with higher w/b ratios, especially Ms0.5 and Ms0.75, experienced a significant extension of the induction period. Consequently, the acceleration peak was not observed in A9 by the end of the measurement

(Figure 4c), leading to a significantly lower 24 h cumulative heat release compared to other AAS mixtures.

Calorimetry findings indicate that increasing water and silicate content might slow down the alkali-activation process. This is due to reduced alkalinity in the pore solution, which decelerated the dissolution of slag particles [40,41]. Aupoil et al. [42] suggested that activators with lower Ms values naturally contain more reactive silicate species to facilitate the alkali activation reaction than those with a higher Ms. In addition, silicate species originating from the activators may inhibit the dissolution of Si from slag particles [43,44], forming a Si-rich layer on the slag surface along with the dissolution of other elements [43,45]. Meanwhile, Ca and Al ions released from slag interact with silicate species in the activator [38], forming primary reaction products that encase the slag particles [46]. These processes may hinder the further ion exchange between undissolved slag grains and the activator solution, leading to a prolonged induction period in high-Ms mixtures. Eventually, the induction phase was terminated as the silicate species from activators were depleted, allowing silicate species from BFS to participate in the activation reaction [46,47].

3.2. Structuration and Workability Retention

The structuration of AAS concrete was indicated by the evolution of static yield stress during the first hour. As illustrated in Figure 5a, the highest initial static yield stress was observed in A1, and it was impossible to perform further tests at later ages. Testing for A2 and A4 was halted after 30 and 45 min, respectively, as the concrete could hardly be remixed thereafter. The red curves in Figure 5a indicate that AAS concretes with a w/b ratio of 0.4 exhibited more rapid structuration within the first hour. It could be inferred that the solid grains were less dispersed in the case of a lower w/b ratio, resulting in stronger particle interactions and increased static yield stress compared to other mixtures. Moreover, the structuration rate decreased with increasing Ms, regardless of the w/b ratio. In the meantime, higher w/b ratios led to a reduction in the slope of the static yield stress curves, consistent with the retarding effects of water and silicate content indicated by calorimetry results. For A9 (Ms0.75, w/b = 0.5), the static yield stress showed only a slight increase during the first hour. The reaction kinetics indicated that the reaction entered an induction stage characterized by a low level of heat flow following the initial dissolution. This suggests that the reaction progressed very slowly during this phase, with the progressive structuration being compromised by the applied shear steps. Notably, a steep build-up process was observed in A2 and A3 after 30 and 45 min, respectively. This aligns with the onset of the acceleration peak in A2 and A3, as illustrated in Figure 4a. The structuration in AAS concrete was enhanced as the exothermic reaction became more pronounced.

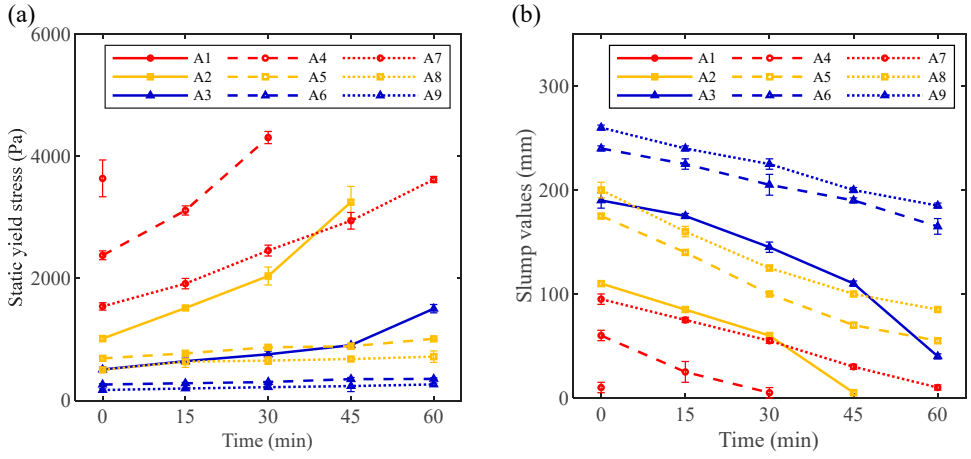

Figure 5. Evolution of (**a**) static yield stress of AAS concretes as a function of time, and (**b**) slump values of AAS concretes as a function of time.

Slump tests were conducted to evaluate the workability retention of AAS concrete, with results shown in Figure 5b. Mixture A9 exhibited higher slump values over time compared to other mixtures. Notably, both A6 and A9 initially achieved the S5 consistency class (EN 206), without noticeable bleeding or segregation. They both maintained a slump of approximately 200 mm by the end of the measurement, indicating good workability retention. In contrast, A2 and A3 experienced a significant slump loss after about 30 and 45 min, respectively, consistent with the static yield stress evolution findings (Figure 5a). Despite all AAS concretes experiencing progressive slump loss over time, some mixtures remained in the induction stage by the end of the measurements. Aside from exothermic chemical reactions, slump loss may also result from non-exothermic reactions, such as floc formation due to colloidal attractions [24,48,49] and close contact interactions [50,51].

3.3. Dynamic Flow Properties

Down-ramp portions of the flow curve in torque-rotational speed relationships are shown in Figure 6. These flow curves were fitted by a Bingham linear model, with all R^2 ranging between 0.9952 and 0.9993. The greatest torque values were detected in A1 with different rotational speeds, resulting in a higher flow curve above the other mixtures. At a fixed w/b of 0.4, the flow curve of AAS concrete moved slightly downward with an increase in Ms (red curves in Figure 6). In the meantime, higher w/b ratios led to more reductions in torque values (solid curves in Figure 6), accompanied by a decreased slope of the flow curves.

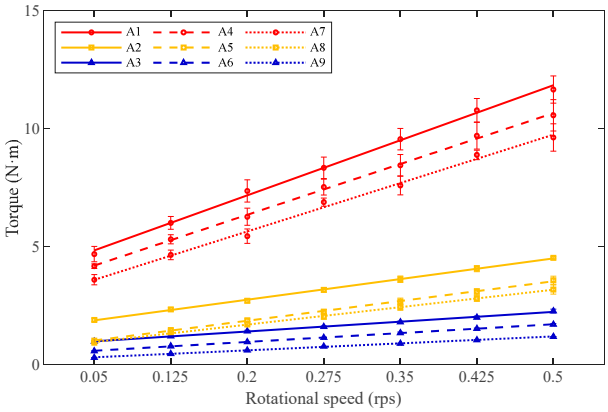

Figure 6. Flow curves of AAS concrete in torque—rotational speed relationships.

The torque–rotational speed data were converted into fundamental rheological parameters (i.e., dynamic yield stress and plastic viscosity) according to Reiner–Riwlin equations, as indicated in Figure 7. The highest dynamic yield stress and plastic viscosity were detected in A1, which contained the lowest water and silicate content among all mixtures. As the w/b ratio increased, both rheological parameters decreased by about 60% and 80% in A2 and A3, respectively. Further, as indicated by the dashed lines in Figure 7, an elevated Ms led to less apparent reductions of rheological parameters than the w/b ratio. Compared with A1, the dynamic yield stress of A4 and A7 decreased by 14.4% and 28.5%, while their plastic viscosity dropped by 7.7% and 12.1%, respectively. The results indicate that the water and silicate in the activator can contribute to a fluidizing effect, enhancing the flowability of AAS concrete. This is ascribed to the increase in the liquid fraction in fresh mixtures. Higher liquid content in the system resulted in more dispersion between solid grains in AAS concrete, which reduced the interparticle frictions and collisions under dynamic flow conditions [52]. Moreover, the liquid phase in the fresh concrete could also fill in the interstitial voids as lubricants to facilitate the flow [53].

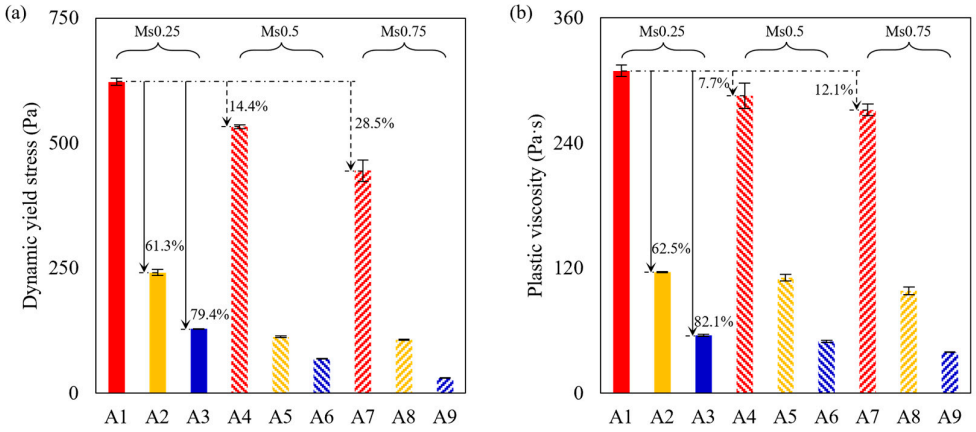

Figure 7. Bingham rheological parameters of AAS concretes: (**a**) dynamic yield stress and (**b**) plastic viscosity.

It is noteworthy that previous studies on AAS paste have reported that the mixtures turned more viscous with higher silicate dosages in the activator [11,54], which is distinct from the results obtained here in AAS concrete. Sodium silicate solutions naturally exhibit higher viscosity with an increased Ms [55,56]. Nevertheless, the AAS concrete viscosity detected in this study is about tens or hundreds of times higher as compared to a typical AAS paste [11], which suggests that the contribution from aggregate fractions might be predominant in concrete flow. In that case, the activator and AAS paste present as the lubricating phase to mitigate the interaction between solid aggregates. Thereby, AAS concrete showed decreased plastic viscosity with an increase of Ms in the activator.

3.4. Thixotropic Behaviors

The thixotropy behavior of AAS concrete was initially evaluated through a stress growth test following a 5 min resting period. The thixotropy index was calculated using Equation (2), and the results are illustrated in Table 4. Among all AAS concretes, A7 exhibited the highest degree of thixotropy, which is approximately three times greater than that of A1. An increase in Ms notably enhanced the thixotropic property of AAS concrete, whereas a higher water content was observed to have a detrimental effect on its thixotropic behavior. For instance, the thixotropic index decreased by 68% and 89% for A8 and A9 compared to A7, respectively.

Table 4. Thixotropic index of AAS concretes obtained from stress growth tests.

Mix	A1	A2	A3	A4	A5	A6	A7	A8	A9
T_I	1.46 ± 0.11	0.73 ± 0.09	0.05 ± 0.01	3.36 ± 0.35	1.31 ± 0.20	0.19 ± 0.02	10.02 ± 0.98	1.83 ± 0.24	0.32 ± 0.04

The maximum and equilibrium torque values (T_m and T_e) for fresh AAS concretes referring to different rotational speeds are summarized in Table 5, and the breakdown areas for different mixtures are illustrated in Figure 8. Increasing the Ms in the activator significantly enhanced thixotropy by raising T_m while slightly decreasing T_e in the mixtures. At 0.6 rps, A7 demonstrated the highest T_m value among all mixtures, outperforming A1 and A4 at the same rotational speed. This suggests that A7 required more shear energy to disrupt interparticle interactions and initiate flow. In the meantime, A7 featured a lower T_e compared to A1 and A4, indicating that less shear energy was needed to maintain equilibrium state flow. Similar outcomes were noted in AAS concretes with higher w/b ratios, aligning with findings from flow curve tests.

Table 5. Maximum and equilibrium torque values determined in AAS concretes by using various rotational speeds.

Torque (Nm)	Mixtures								
	A1	**A2**	**A3**	**A4**	**A5**	**A6**	**A7**	**A8**	**A9**
T_m (0.15 rps)	12.63	3.59	1.41	20.23	4.32	1.42	28.01	6.2	3.25
T_m (0.3 rps)	15.99	4.36	1.86	20.58	7.8	2.11	29.23	9.03	3.26
T_m (0.45 rps)	19.64	5.45	2.04	21.44	8.67	2.33	30.92	10.2	3.44
T_m (0.6 rps)	20.31	6.5	2.08	23.26	9.66	2.54	31.75	10.59	4
T_e (0.15 rps)	6.04	2.32	0.64	6.04	1.76	0.61	5.35	1.33	0.6
T_e (0.3 rps)	8.23	3.15	1.03	7.8	2.31	0.94	7.4	2.03	0.89
T_e (0.45 rps)	9.77	3.94	1.23	8.93	2.97	1.19	8.61	2.49	1.08
T_e (0.6 rps)	10.28	4.27	1.47	9.76	3.27	1.36	9.32	2.89	1.26

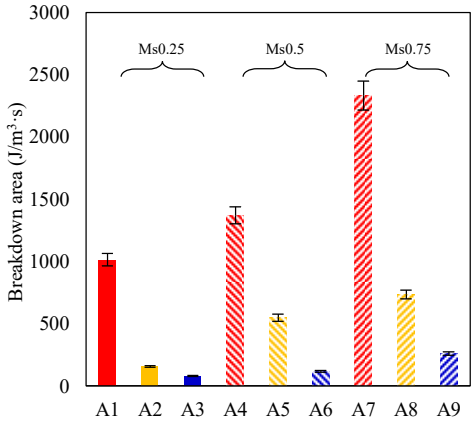

Figure 8. Breakdown area of AAS concretes by using various rotational speeds.

By contrast, both T_m and T_e values significantly dropped with a higher w/b ratio, weakening the thixotropic properties of AAS concrete. The dilution from the extra water decreased the alkalinity in the pore solution, likely attenuating the dissolution of slag particles. Further, the increase in water content led to a better dispersion of solid particles from each other. As a result, more reaction products are needed to undertake interparticle interactions, which accounts for the diminished thixotropic behavior.

In addition, the thixotropy of the AAS mixture was further assessed by the drop in apparent viscosity, as presented in Table 6. At a fixed rotational speed, it was found that the variation in Δ_{app} values followed a similar trend as the thixotropic index and the breakdown area derived above. Furthermore, Figure 9 presents the relationships among the results from various methods, in which strong correlations were identified, yielding an R^2 of around 0.9. This suggests that both methods could reliably estimate the thixotropy of AAS concrete. Comparatively, the thixotropic index and drop in apparent viscosity could be applied as a simple testing method for practical applications, while the breakdown area gives more accurate results to evaluate the thixotropy as it considers the result measured from various shear speeds.

Table 6. Drop in apparent viscosity of AAS concretes under different rotational speeds.

Δ_{app} (Pa·s)	**A1**	**A2**	**A3**	**A4**	**A5**	**A6**	**A7**	**A8**	**A9**
N = 0.15 rps	1505	467	167	2931	414	160	4540	918	545
N = 0.3 rps	887	241	100	1276	481	112	2215	694	240
N = 0.45 rps	760	204	66	804	325	76	1584	498	155
N = 0.6 rps	568	187	43	670	279	55	1187	378	137

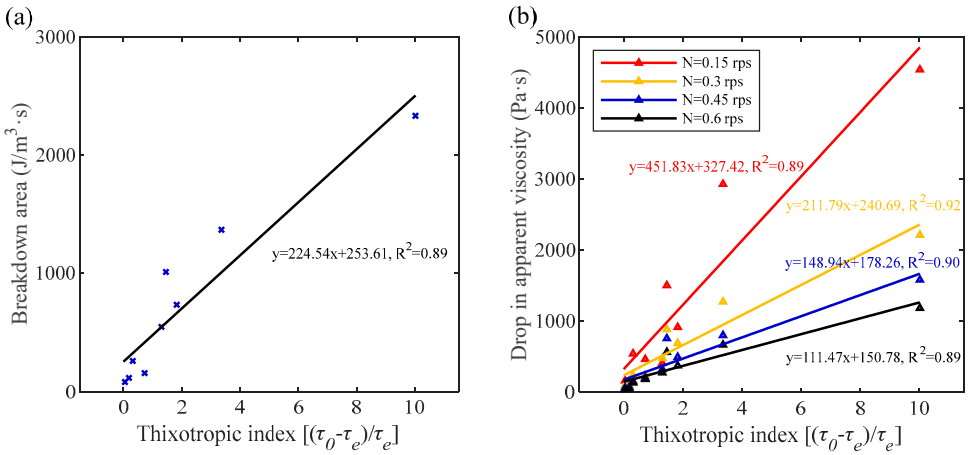

Figure 9. Correlation between the thixotropic parameters of AAS concrete. (**a**) Breakdown area against thixotropic index. (**b**) Drop in apparent viscosity against thixotropic index.

4. Discussion

The thixotropy of PC materials is attributed to colloidal coagulations and interparticle interactions, through the percolation of initial hydration products like C-S-H and ettringite [24,26]. In AAS, however, the silicate species within the activator present as interparticle gels, promoting the dispersion of solid grains [57]. By adopting sodium silicate activators, a few studies reported that the interparticle colloidal interactions were hardly detected due to the predominance of a viscous effect instead [11,13]. Thus, the microstructural characteristics indicate that a higher silicate concentration in the activator could reduce the thixotropic behavior of AAS concrete, which contradicts the findings in Table 4.

On top of that, the time-dependent behavior of chemical reactions during rest also significantly influences the thixotropy of cementitious composites. Previous studies on AAMs have shown that silicate species in activators may act as nucleation sites, facilitating the accumulation of reaction product nuclei within the liquid phase [58,59]. As reported in [38], the AAS mixtures with high Ms were featured with an elevated initial reactivity and rapid precipitation of early hydration products. Consequently, the binding phase experienced a substantial increment in the volume fraction and surface area, enhancing the interparticle interactions between precursor grains [26]. This is in line with the principle of accelerating additives applied in PC binders, i.e., the thixotropic property is improved by forming large numbers of fine particles [39,60]. Therefore, greater shear energy is needed to disrupt the agglomeration of solid grains in AAS concrete with higher Ms and initiate the flow. Furthermore, Duxson et al. [61] suggested that the number of oligomers and polymeric silicate species is proportional to the Ms value of activator solutions. By contrast, monomeric and dimeric species were more detected with the reduction in Ms [62,63]. As reported in [39], the presence of long-chain polymer structures in activators may enhance the cohesiveness of the material while at rest, attributed to their entanglement and association. Consequently, A7, A8, and A9 demonstrated more significant thixotropic behaviors, notably exhibiting a higher T_m compared to other mixtures with an identical w/b ratio (Table 5).

On the other hand, AAS concretes with a higher Ms exhibited a lower T_e at equilibrium, depicted in Table 5. It can be inferred that the cohesive effect of entangled oligomers and polymers was eliminated once flow began, as their spatial arrangement aligned with the shear direction. Additionally, the flocculated frameworks through early reaction products were progressively broken into finer particles due to applied shear energy [26], which could fill interstitial voids and act as lubricants around solid grains [64]. Furthermore, the increase in silicate content in the activator may improve the dispersion of solid grains, enhancing fluidity in dynamic flows [57,65]. Consequently, lower shear energy is needed to sustain an equilibrium flow.

From the mix design point of view, the influence of aggregate content should be considered as well. Previous studies have reported that aggregates may contribute to more internal frictions/collisions and greater resistance to initiate the flow, leading to a stronger thixotropy [26]. In this study, the precursor content was kept constant among AAS concretes, while the variation per unit volume by applying different alkali dosages was compensated by aggregates. Results show that A4 and A7 consisting of less aggregate exhibited a higher degree of thixotropy as compared to A1. It can be deduced that the slight reduction in aggregate content was shaded by the strong effect of Ms on the thixotropic build-up. Moreover, A2 and A3 showed much less thixotropy than A1, indicating that the reduction in aggregate content might be influential as well, in addition to higher w/b ratios.

In summary, the early-stage structuration in AAS concrete can be categorized into different mechanisms, ascribed to the distinct features of microstructure development with the variation in activator compositions [66]. Mixtures with lower Ms showed rapid build-up, inclined to be an irreversible evolution, which is associated with the early onset of acceleration stage reactions. In contrast, higher Ms in the activator enhanced the thixotropic behavior of AAS concrete at early ages, which was largely reversible and irrelevant to the acceleration stage reactions. Once the thixotropy was eliminated, high-Ms AAS concrete preserved good flow properties due to the dispersing effects of silicate species in activators [38]. Likewise, a longer mixing time has been reported to be effective in maintaining the workability of AAS mixtures [16,54,67].

5. Conclusions

This study comprehensively investigates the flow properties and thixotropy of AAS concretes with various silicate modulus (Ms) and water-to-binder (w/b) ratios. In addition, reaction kinetics have been evaluated as a function of time. The following conclusions can be drawn:

- The dynamic flow properties of AAS concrete improved with an increase in Ms and w/b ratios in the activator. A higher Ms led to a reduction in viscosity, which contrasts with observations at the paste level. This suggests that aggregates play a more significant role in influencing the rheology of AAS concrete.
- An increase in Ms significantly enhanced the thixotropic properties of AAS concrete. For mixtures with a w/b ratio of 0.4, the maximum torque (at 0.6 rps) from a static state increased by 56.3% when Ms rose from 0.25 to 0.75. This enhancement was accompanied by slight reductions in equilibrium torque values. However, as the w/b ratio increased, thixotropic properties gradually diminished.
- The thixotropic behavior of AAS concrete was assessed through multiple methods. A linear correlation was observed between the degree of thixotropy and the breakdown area determined under static and dynamic equilibrium flow conditions of AAS concretes. Additionally, the thixotropic index exhibited a linear relationship with the drop in apparent viscosity, which diminished as the rotational speed increased.
- AAS concrete with lower w/b ratios and Ms exhibited faster slump loss and irreversible structuration, attributed to the early onset of acceleration stage reactions identified through calorimetry. Conversely, AAS concrete with higher Ms demonstrated better flowability and workability retention within the first hour after eliminating thixotropic build-up, aligning with the extended induction period observed.

Author Contributions: J.Z. (Jian Zhang): Conceptualization, Methodology, Investigation, Writing—original draft; Y.L.: Methodology, Investigation, Writing—original draft; J.Z. (Jin Zhu): Investigation, Writing—review and editing; J.L.: Writing—review and editing; Y.M.: Writing—review and editing; S.Z.: Funding acquisition, Investigation, Writing—review and editing; Y.S.: Funding acquisition, Writing—review and editing. All authors have read and agreed to the published version of the manuscript.

Funding: This research was funded by the National Natural Science Foundation of China (No. 52408279) and (No.52308246), the Major Program of the National Natural Science Foundation of

China (No. 52090084), the State Key Program of the National Natural Science Foundation of China (Grant No. 51938008) and the State Key Laboratory of High Performance Civil Engineering Materials (No. 2023CEM009).

Data Availability Statement: Data are contained within the article.

Conflicts of Interest: The authors declare no conflict of interest.

References

1. Duxson, P.; Brice, D.G. Chemical Research and Climate Change as Drivers in the Commercial Adoption of Alkali Activated Materials. *Waste Biomass Valorization* **2010**, *1*, 145–155. [CrossRef]
2. Provis, J.L.; Van Deventer, J.S.J. *Alkali Activated Materials: State-of-the-Art Report, RILEM TC 224-AAM*; Springer Science & Business Media: Berlin/Heidelberg, Germany, 2013.
3. Turner, L.K.; Collins, F.G. Carbon dioxide equivalent (CO2-e) emissions: A comparison between geopolymer and OPC cement concrete. *Constr. Build. Mater.* **2013**, *43*, 125–130. [CrossRef]
4. Chen, C.; Habert, G.; Bouzidi, Y.; Jullien, A. Environmental impact of cement production: Detail of the different processes and cement plant variability evaluation. *J. Clean. Prod.* **2010**, *18*, 478–485. [CrossRef]
5. Gong, M.; Li, M.; Wang, W.; Tan, Z.; Sun, Y. Investigation of micromechanics and relaxation spectrum evolution in multiple recycled asphalt binders. *Mater. Struct.* **2024**, *57*, 165. [CrossRef]
6. Zhong, M.; Meng, J.; Ning, B.; Na, F.; Cui, T.; Shi, X.; Cui, T. Preparation and alkali excitation mechanism of coal gangue-iron ore tailings non-sintering ceramsite. *Constr. Build. Mater.* **2024**, *426*, 136209. [CrossRef]
7. Luukkonen, T.; Abdollahnejad, Z.; Yliniemi, J.; Kinnunen, P.; Illikainen, M. One-part alkali-activated materials: A review. *Cem. Concr. Res.* **2018**, *103*, 21–34. [CrossRef]
8. Provis, J.L. Geopolymers and other alkali activated materials: Why, how, and what? *Mater. Struct. Constr.* **2014**, *47*, 11–25. [CrossRef]
9. Aiken, T.A.; Sha, W.; Kwasny, J.; Soutsos, M.N. Cement and Concrete Research Resistance of geopolymer and Portland cement based systems to silage ef fl uent attack. *Cem. Concr. Res.* **2017**, *92*, 56–65. [CrossRef]
10. Jansson, H.; Bernin, D.; Ramser, K. Silicate species of water glass and insights for alkali-activated green cement. *AIP Adv.* **2015**, *5*, 067167. [CrossRef]
11. Alnahhal, M.F.; Kim, T.; Hajimohammadi, A. Distinctive rheological and temporal viscoelastic behaviour of alkali-activated fly ash/slag pastes: A comparative study with cement paste. *Cem. Concr. Res.* **2021**, *144*, 106441. [CrossRef]
12. Lu, C.; Zhang, Z.; Shi, C.; Li, N.; Jiao, D.; Yuan, Q. Rheology of alkali-activated materials: A review. *Cem. Concr. Compos.* **2021**, *121*, 104061. [CrossRef]
13. Favier, A.; Hot, J.; Habert, G.; Roussel, N.; D'Espinose De Lacaillerie, J.B. Flow properties of MK-based geopolymer pastes. A comparative study with standard Portland cement pastes. *Soft Matter.* **2014**, *10*, 1134–1141. [CrossRef] [PubMed]
14. Palacios, M.; Puertas, F. Effect of superplasticizer and shrinkage-reducing admixtures on alkali-activated slag pastes and mortars. *Cem. Concr. Res.* **2005**, *35*, 1358–1367. [CrossRef]
15. Criado, M.; Palomo, A.; Fernández-Jiménez, A.; Banfill, P.F.G. Alkali activated fly ash: Effect of admixtures on paste rheology. *Rheol. Acta.* **2009**, *48*, 447–455. [CrossRef]
16. Puertas, F.; González-Fonteboa, B.; González-Taboada, I.; Alonso, M.M.; Torres-Carrasco, M.; Rojo, G.; Martínez-Abella, F. Alkali-activated slag concrete: Fresh and hardened behaviour. *Cem. Concr. Compos.* **2018**, *85*, 22–31. [CrossRef]
17. Laskar, A.I.; Bhattacharjee, R. Rheology of Fly-Ash-Based Geopolymer Concrete. *ACI Mater. J.* **2011**, *108*, 536.
18. Jiao, D.; De Schryver, R.; Shi, C.; De Schutter, G. Thixotropic structural build-up of cement-based materials: A state-of-the-art review. *Cem. Concr. Compos.* **2021**, *122*, 104152. [CrossRef]
19. Wallevik, J.E. Rheological properties of cement paste: Thixotropic behavior and structural breakdown. *Cem. Concr. Res.* **2009**, *39*, 14–29. [CrossRef]
20. Jiao, D.; Shi, C.; Yuan, Q.; An, X.; Liu, Y.; Li, H. Effect of constituents on rheological properties of fresh concrete—A review. *Cem. Concr. Compos.* **2017**, *83*, 146–159. [CrossRef]
21. Mewis, J.; Wagner, N.J. Thixotropy. *Adv. Colloid Interface Sci.* **2009**, *147–148*, 214–227. [CrossRef]
22. Roussel, N.; Le Roy, R.; Coussot, P. Thixotropy modelling at local and macroscopic scales. *J. Non-Newton. Fluid Mech.* **2004**, *117*, 85–95. [CrossRef]
23. Roussel, N. A thixotropy model for fresh fluid concretes: Theory, validation and applications. *Cem. Concr. Res.* **2006**, *36*, 1797–1806. [CrossRef]
24. Roussel, N.; Ovarlez, G.; Garrault, S.; Brumaud, C. The origins of thixotropy of fresh cement pastes. *Cem. Concr. Res.* **2012**, *42*, 148–157. [CrossRef]
25. Wallevik, J.E. Thixotropic investigation on cement paste: Experimental and numerical approach. *J. Non-Newton. Fluid Mech.* **2005**, *132*, 86–99. [CrossRef]
26. Ahari, R.S.; Erdem, T.K.; Ramyar, K. Thixotropy and structural breakdown properties of self consolidating concrete containing various supplementary cementitious materials. *Cem. Concr. Compos.* **2015**, *59*, 26–37. [CrossRef]

27. Khayat, K.H.; Saric-Coric, M.; Liotta, F. Influence of thixotropy on stability characteristics of cement grout and concrete. *ACI Mater. J.* **2002**, *99*, 234–241. [CrossRef]
28. Assaad, J.; Khayat, K.H.; Mesbah, H. Variation of Formwork Pressure with Thixotropy of Self-Consolidating Concrete Variation of Formwork Pressure with Thixotropy of Self-Consolidating Concrete. *Mater. J.* **2003**, *100*, 29–37.
29. Khayat, K.H.; Assaad, J. Assessment of Thixotropy of Self- Consolidating Concrete and Concrete-Equivalent-Mortar—Effect of Binder Composition and Content. *ACI Mater. J.* **2004**, *101*, 400–408.
30. Feys, D.; Verhoeven, R.; De Schutter, G. Influence of thixotropy on pressures required during pumping of concrete. In Proceedings of the 15th International Congress on Rheology and 80th Annual Meeting of the Society-of-Rheology, Monterey, CA, USA, 3–8 August 2008; American Institute of Physics: College Park, MD, USA, 2008; pp. 710–712.
31. Roussel, N.; Cussigh, F. Distinct-layer casting of SCC: The mechanical consequences of thixotropy. *Cem. Concr. Res.* **2008**, *38*, 624–632. [CrossRef]
32. Reiter, L.; Wangler, T.; Roussel, N.; Flatt, R.J. The role of early age structural build-up in digital fabrication with concrete. *Cem. Concr. Res.* **2018**, *112*, 86–95. [CrossRef]
33. Mechtcherine, V.; Bos, F.P.; Perrot, A.; da Silva, W.R.L.; Nerella, V.N.; Fataei, S.; Wolfs, R.J.M.; Sonebi, M.; Roussel, N. Extrusion-based additive manufacturing with cement-based materials–production steps, processes, and their underlying physics: A review. *Cem. Concr. Res.* **2020**, *132*, 106037. [CrossRef]
34. Zhang, S.; Li, Z.; Ghiassi, B.; Yin, S.; Ye, G. Fracture properties and microstructure formation of hardened alkali-activated slag/fly ash pastes. *Cem. Concr. Res.* **2021**, *144*, 106447. [CrossRef]
35. Favier, A.; Habert, G.; D'Espinose De Lacaillerie, J.B.; Roussel, N. Mechanical properties and compositional heterogeneities of fresh geopolymer pastes. *Cem. Concr. Res.* **2013**, *48*, 9–16. [CrossRef]
36. Koehler, E.P.; Fowler, D.W. *Development of a Portable Rheometer for Fresh Portland Cement Concrete*; University of Texas at Austin: Austin, TX, USA, 2004.
37. Feys, D.; Wallevik, J.E.; Yahia, A.; Khayat, K.H.; Wallevik, O.H. Extension of the Reiner-Riwlin equation to determine modified Bingham parameters measured in coaxial cylinders rheometers. *Mater. Struct. Constr.* **2013**, *46*, 289–311. [CrossRef]
38. Palacios, M.; Gismera, S.; Alonso, M.M.; Espinose, J.B.; Lacaillerie, D.; Lothenbach, B.; Favier, A.; Brumaud, C.; Puertas, F. Cement and Concrete Research Early reactivity of sodium silicate-activated slag pastes and its impact on rheological properties. *Cem. Concr. Res.* **2021**, *140*, 106302. [CrossRef]
39. Assaad, J.; Khayat, K.H.; Mesbah, H. Assessment of thixotropy of flowable and self-consolidating concrete. *ACI Mater. J.* **2003**, *100*, 99–107. [CrossRef]
40. Chang, J.-J. A study on the setting characteristics of sodium silicate-activated slag pastes. *Cem. Concr. Res.* **2003**, *33*, 1005–1011. [CrossRef]
41. Ravikumar, D.; Neithalath, N. Reaction kinetics in sodium silicate powder and liquid activated slag binders evaluated using isothermal calorimetry. *Thermochim. Acta.* **2012**, *546*, 32–43. [CrossRef]
42. Aupoil, J.; Champenois, J.-B.; d'Espinose de Lacaillerie, J.-B.; Poulesquen, A. Interplay between silicate and hydroxide ions during geopolymerization. *Cem. Concr. Res.* **2019**, *115*, 426–432. [CrossRef]
43. Zuo, Y.; Ye, G. Preliminary interpretation of the induction period in hydration of sodium hydroxide/silicate activated slag. *Materials* **2020**, *13*, 4796. [CrossRef]
44. Duxson, P.; Provis, J.L. Designing precursors for geopolymer cements. *J. Am. Ceram. Soc.* **2008**, *91*, 3864–3869. [CrossRef]
45. Zhang, X.; Sun, Y.; Zhang, Q.; Tian, W.; Khan, E.; Tsang, D.C.W. Leaching characteristics of nutrients in food waste digestate-derived biochar. *Bioresour. Technol.* **2024**, *399*, 130634. [CrossRef] [PubMed]
46. Cao, R.; Zhang, S.; Banthia, N.; Zhang, Y.; Zhang, Z. Interpreting the early-age reaction process of alkali-activated slag by using combined embedded ultrasonic measurement, thermal analysis, XRD, FTIR and SEM. *Compos. Part B Eng.* **2020**, *186*, 107840. [CrossRef]
47. Puertas, F.; Fernández-Jiménez, A.; Blanco-Varela, M.T. Pore solution in alkali-activated slag cement pastes. Relation to the composition and structure of calcium silicate hydrate. *Cem. Concr. Res.* **2004**, *34*, 139–148. [CrossRef]
48. Qian, Y.; Lesage, K.; El Cheikh, K.; De Schutter, G. Effect of polycarboxylate ether superplasticizer (PCE) on dynamic yield stress, thixotropy and flocculation state of fresh cement pastes in consideration of the Critical Micelle Concentration (CMC). *Cem. Concr. Res.* **2018**, *107*, 75–84. [CrossRef]
49. Roussel, N.; Bessaies-Bey, H.; Kawashima, S.; Marchon, D.; Vasilic, K.; Wolfs, R. Recent advances on yield stress and elasticity of fresh cement-based materials. *Cem. Concr. Res.* **2019**, *124*, 105798. [CrossRef]
50. Roussel, N.; Lemaître, A.; Flatt, R.J.; Coussot, P. Steady state flow of cement suspensions: A micromechanical state of the art. *Cem. Concr. Res.* **2010**, *40*, 77–84. [CrossRef]
51. Zhu, J.; Liu, J.; Khayat, K.H.; Shu, X.; Ran, Q.; Li, Z. Mechanisms affecting viscosity of cement paste made with microfines of manufactured sand. *Cem. Concr. Res.* **2022**, *156*, 106757. [CrossRef]
52. Khayat, K.H.; Yahia, A. Effect of welan gum-high-range water reducer combinations on rheology of cement grout. *Mater. J.* **1997**, *94*, 365–372.
53. Hajar, Z.; Resplendino, J.; Lecointre, D.; Petitjean, J.; Simon, A. Ultra-high-performance concretes: First recommendations and examples of application. In Proceedings of the Infib Symposium, Avignon, France, 26–28 April 2004.

54. Puertas, F.; Varga, C.; Alonso, M.M. Rheology of alkali-activated slag pastes. Effect of the nature and concentration of the activating solution. *Cem. Concr. Compos.* **2014**, *53*, 279–288. [CrossRef]
55. Yang, X.; Zhu, W.; Yang, Q. The viscosity properties of sodium silicate solutions. *J. Solution Chem.* **2008**, *37*, 73–83. [CrossRef]
56. Zhang, X.; Chen, Z.; Kang, J.; Zhao, S.; Wang, B.; Yan, P.; Deng, F.; Shen, J.; Chu, W. UV/peroxymonosulfate process for degradation of chloral hydrate: Pathway and the role of radicals. *J. Hazard. Mater.* **2021**, *401*, 123837. [CrossRef] [PubMed]
57. Sun, Y.; Zhang, S.; Rahul, A.V.; Tao, Y.; Van Bockstaele, F.; Dewettinck, K.; Ye, G.; De Schutter, G. Rheology of alkali-activated slag pastes: New insight from microstructural investigations by cryo-SEM. *Cem. Concr. Res.* **2022**, *157*, 106806. [CrossRef]
58. Hubler, M.H.; Thomas, J.J.; Jennings, H.M. Influence of nucleation seeding on the hydration kinetics and compressive strength of alkali activated slag paste. *Cem. Concr. Res.* **2011**, *41*, 842–846. [CrossRef]
59. Gebregziabiher, B.S.; Thomas, R.; Peethamparan, S. Very early-age reaction kinetics and microstructural development in alkali-activated slag. *Cem. Concr. Compos.* **2015**, *55*, 91–102. [CrossRef]
60. Wang, W.; Sun, L.; Li, M.; Cheng, H.; Gong, M.; Sun, Y.; Cheng, Z.; Xie, S. Mechanical Properties and Micromechanisms of SBS-Modified Asphalt Binder under Multiple Aging and Regeneration Effects. *J. Mater. Civ. Eng.* **2024**, *36*, 4024284. [CrossRef]
61. Duxson, P.; Provis, J.L.; Lukey, G.C.; Mallicoat, S.W.; Kriven, W.M.; Van Deventer, J.S.J. Understanding the relationship between geopolymer composition, microstructure and mechanical properties. *Colloids Surf. A Physicochem. Eng. Asp.* **2005**, *269*, 47–58. [CrossRef]
62. Svensson, I.L.; Sjöberg, S.; Öhman, L.-O. Polysilicate equilibria in concentrated sodium silicate solutions. *J. Chem. Soc. Faraday Trans. 1 Phys. Chem. Condens. Phases* **1986**, *82*, 3635–3646. [CrossRef]
63. Zhang, X.; Kang, J.; Chu, W.; Zhao, S.; Shen, J.; Chen, Z. Spectral and mass spectrometric characteristics of different molecular weight fractions of dissolved organic matter. *Sep. Purif. Technol.* **2020**, *253*, 117390. [CrossRef]
64. Tattersall, G.H.; Banfill, P.F.G. *The Rheology of Fresh Concrete*; Pitman Books Limited: Bath, UK, 1983.
65. Alonso, M.M.; Gismera, S.; Blanco, M.T.; Lanzón, M.; Puertas, F. Alkali-activated mortars: Workability and rheological behaviour. *Constr. Build. Mater.* **2017**, *145*, 576–587. [CrossRef]
66. Sun, Y.; Miranda, L.; Lima, D.; Rossi, L.; Jiao, D.; Li, Z.; Ye, G.; De Schutter, G. Cement and Concrete Research Interpretation of the early stiffening process in alkali-activated slag pastes. *Cem. Concr. Res.* **2023**, *167*, 107118. [CrossRef]
67. Palacios, M.; Puertas, F. Effectiveness of mixing time on hardened properties of waterglass-activated slag pastes and mortars. *ACI Mater. J.* **2011**, *108*, 73.